PERGAMON

Solid-State Electronics 44 (2000) 703–711

SOLID-STATE ELECTRONICS

Microelectronic circuit characterization via photothermal radiometry of scribeline recombination lifetime

M.E. Rodriguez[a,*,1], A. Mandelis[a], G. Pan[a], J.A. Garcia[a], Y. Riopel[b]

[a]Photothermal and Optoelectronic Diagnostics Laboratories (PODL), Department of Mechanical and Industrial Engineering, University of Toronto and Materials and Manufacturing Ontario, 5 King's College Road, Toronto, Ontario, Canada, M5 S 3G8
[b]MITEL SCC, 18 Boul. De l'Aeroport, Bromont, Quebec, Canada, JOE 1LO

Received 10 September 1999; accepted 13 October 1999

Abstract

Three-dimensional (3D) photothermal radiometric microscopic imaging and laser-intensity-modulation frequency scans have been used for the non-contact, non-intrusive measurement of electronic transport properties of integrated circuits in patterned 4″ Si wafers. The experimental data showed that carrier recombination lifetimes along each scribeline remain constant. However, variations in surface recombination velocities and carrier diffusion coefficients were found. It was further found that such variations are related to the presence of highly doped poly-Si structures adjacent to the scribeline. As a result of these measurements, it is concluded that scribeline photothermal radiometric probing can be used effectively for monitoring local values of the carrier recombination lifetime and, through those, wafer contamination and damage during device fabrication processing.

1. Introduction

There are four basic operations performed on a wafer during the fabrication process: layering, patterning, doping and heat treating/oxidation. Layering is the operation used to add thin layers to the wafer surface. These layers are insulators, semiconductors or conductors including interconnects; they are made of different materials and are grown or deposited by a variety of techniques [1]. Patterning is the series of steps that results in the removal of selected portions of the added layers. This process is also known as photomasking, masking, photolithography, and microlithography. It is the patterning operation that creates the surface parts of the device that make up a circuit. This operation sets the critical dimensions of devices. Errors in the patterning process can cause changes in the electrical functionality of the devices and of the circuit. Contamination in any and all of the process steps can introduce defects and/or electrical faults leading to device failure. Contamination problems tend to be magnified by the fact that patterning operations are performed on the wafer several times in the course of the wafer fabrication process.

In recent years the laser photothermal radiometric (PTR) technique has been under development in our laboratory and elsewhere to perform non-contact, remote measurements of electronic transport properties of industrial Si wafers [2]. Several recent studies [3–5]

* Corresponding author. Tel.: +1-416-978-1287.
E-mail address: mario@mie.utoronto.ca (M.E. Rodriguez).
[1] On leave from: Centro de Investigacion en Ciencia Aplicada y Tecnologia Avanzada del I.P.N. Unidad Queretaro, Jose siurob 10, Col. Alamedas, Queretaro, Mexico

0038-1101/00/$ - see front matter
PII: S0038-1101(99)00289-0

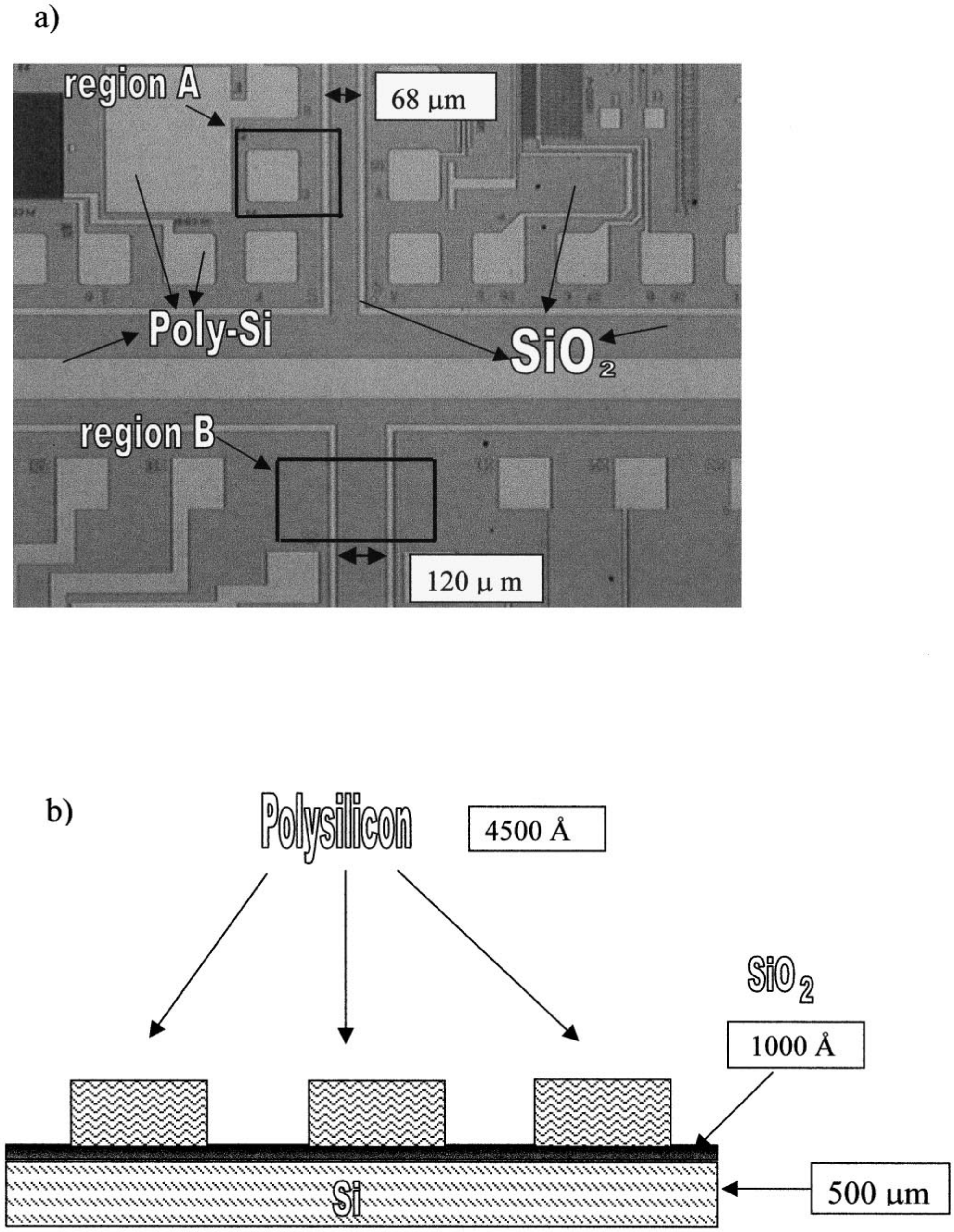

Fig. 1. (a) Microscope photograph showing two different sizes of scribelines in a patterned wafer. (b) Schematic representation of the cross-sectional geometry of the wafers.

have been reported, where measurements of carrier recombination lifetime, surface recombination velocity, electronic and thermal diffusivity, were successfully carried out on 4″ and 6″ Si wafers by means of PTR. Regarding the monitoring of photoexcited free carrier plasmas, PTR was found to be a technique of superior sensitivity to the commercially available photomodulated thermoreflectance (PMOR) technique [6]. In one wafer contamination study [5], the carrier recombination lifetime was found to depend on the number of chemical cleans to which a wafer was exposed. Very recently, an extensive series of PTR studies was made

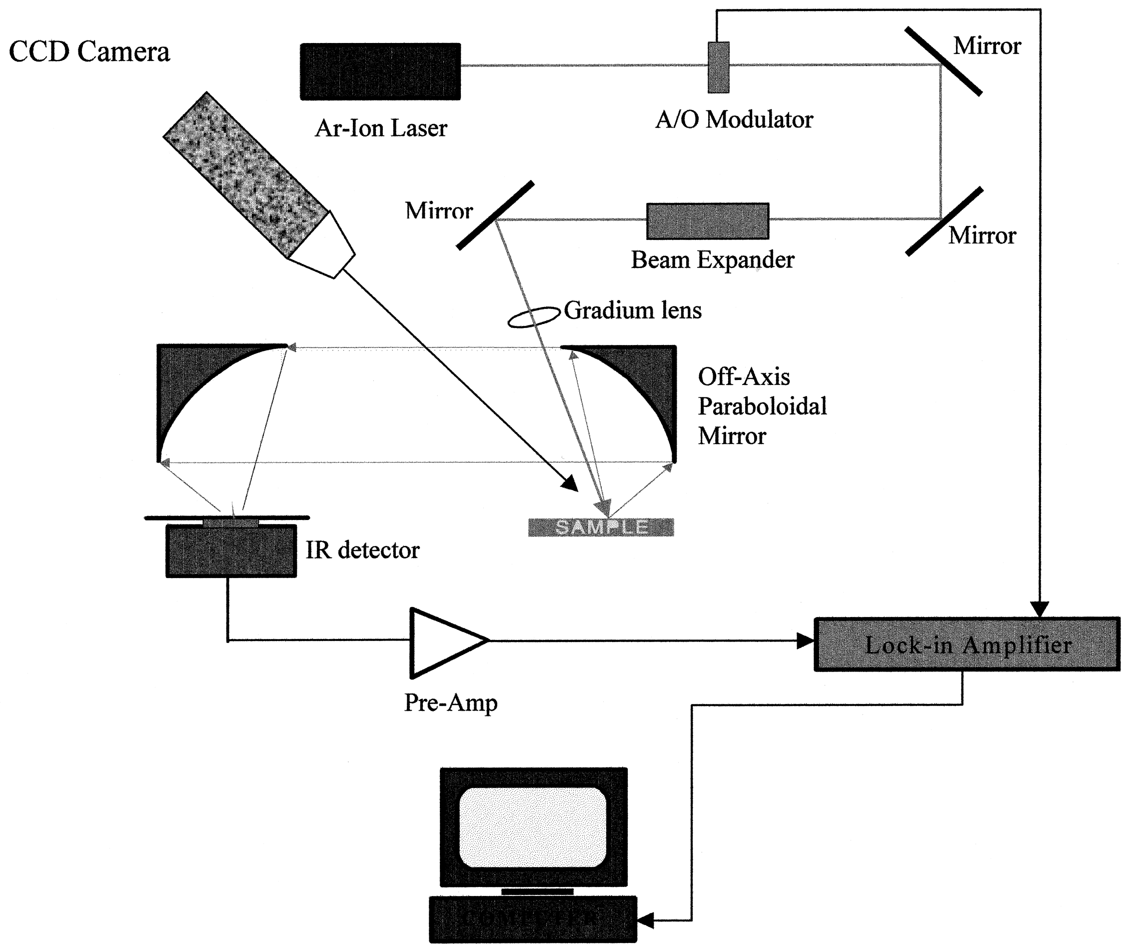

Fig. 2. Experimental setup for the 3D-PTR measurements.

on recombination lifetimes and surface recombination velocities of 36 thermally oxidized 6″ wafers of p-type Si of two different resistivities [7]. The wafers were processed and thermally (isochronally) annealed using a horizontal furnace type BDF-200. The major outcomes of that study were the introduction of a robust computational method based on a multi-parameter-fit algorithm for the measurement of the carrier transport properties (recombination lifetime, front and back surface recombination velocities, electronic and thermal diffusivities); and a strong correlation between resistivity, front-surface recombination velocity and lifetime. The processed higher resistivity wafers were likely to have lower front-surface recombination velocity, S_1, and higher lifetime, τ. Therefore, the values of these parameters are considered to be good benchmarks for monitoring furnace contamination by heavy metals and other agents during processing.

There is a demonstrated need for convenient, effective and efficient monitoring of wafer electronic transport properties, in a non-contact manner throughout the device fabrication process. Wafer contamination diagnostics (including laser PTR), however, may be difficult to apply in the presence of processed devices, metallization layers, interconnects and high-density circuits, which are common in today's microelectronics technologies (e.g. CMOS). To avoid such difficulties, scribeline PTR measurements away from active or passive device structures may offer a viable alternative for monitoring contamination in processed wafers. This paper is focused on scribeline studies of electronic and thermal parameters of various 4″ Si wafers with patterned microelectronic circuits, using 3D PTR microscopic imaging and frequency scans. Special attention was paid to the influence on the transport parameters of poly-Si structures adjacent to scribelines.

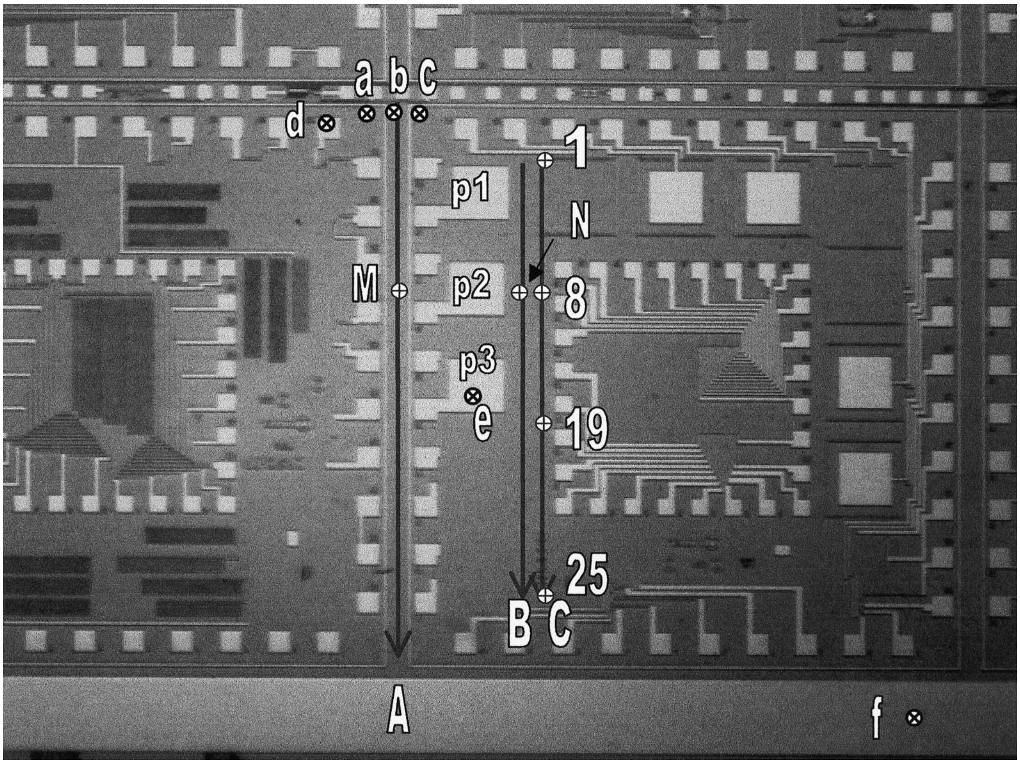

Fig. 3. Microscope photograph of a characteristic region located 2 cm away from the wafer flat, showing the topology of PTR line scans.

2. Sample description

The samples used in this work were four 4″ wafers of p-type Si, with patterned device structures. The wafers had been oxidized with a 1000-Å gate oxide. Polycrystalline Si (polysilicon) was deposited and patterned to form pads of different sizes and shapes. Fig. 1(a) shows an optical microscope photograph of two different sizes of scribelines. One type of scribeline was 120 μm in width; the other type was about 68 μm wide. Throughout this work, bright structures in photographs are (light scattering) poly-Si pads or devices, whereas darker regions are the more highly reflecting SiO_2–Si interfaces. Fig. 1(b) is a schematic of the cross-sectional geometry of the wafer. The poly-Si layer thickness was about 4500 Å.

3. Experimental setup and methodology

The experimental set-up used for frequency scan probing and thermoelectronic imaging inside and outside scribelines is shown in Fig. 2 and has been described elsewhere [3,7,8]. For this study the spot size of the exciting beam was controlled by using a gradium lens (12.5-cm working distance). The excitation beam was modulated from 10 Hz to 100 kHz via an acousto-optic modulator (AOM). The infrared (IR) emission was collected by two collimating off-axis paraboloidal mirrors and was focused onto a liquid- nitrogen-cooled HgCdTe (MCT) IR detector with spectral response between 2 and 12 μm. The PTR signal from the amplifier was fed into a lock-in amplifier and was processed by a personal computer.

Radiometric images were generated using a manual scanning system. These images are PTR amplitude and phase scans at a fixed laser-beam-intensity modulation frequency. In recent work we have shown that the amplitude scales linearly with the recombination lifetime in some ranges of parameters [7]. Therefore, an x–y amplitude scan of Si substrate (with or without the presence of oxide) when it is properly calibrated in units of μs, yields, in principle, a recombination lifetime image of the scanned region. Such a radiometric image has been called a “thermoelectronic image”, or “thermoelectronic scan”. The resolution of each spot was 20 μm. Beam size was estimated to be 48 μm using a CCD camera and optical scan measurements through a 5-μm pinhole. The laser power on the wafer was about 40 mW, which corresponds to a low injec-

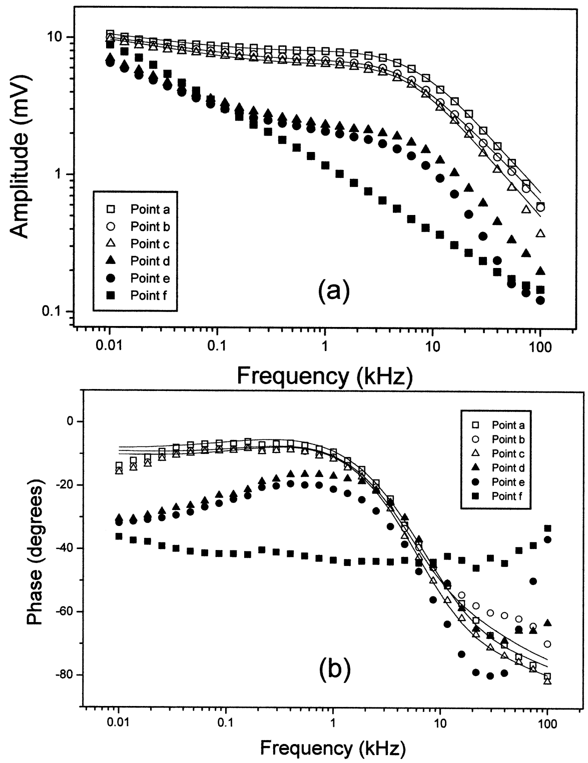

Fig. 4. PTR signal amplitude (a) and phase (b) for six positions (three SiO_2 and three poly-Si pads) shown in Fig. 3.

tion level. On scanning across typical wafer structures shown in Fig. 1, the CCD camera was used to determine the desired location and to guide the laser beam inside or around the neighborhood of a given scribeline.

4. Results and discussion

4.1. Frequency scans

The sample wafers were scanned along and across a scribeline, through poly-Si and oxide-covered regions. Fig. 3 shows the topology of a typical small area near the crossing of two scribelines, one of which contains test inserts. Frequency scans were carried out at six locations (a)–(f): three (a)–(c) across the insert-free scribeline (120-μm-wide) very near the crossing point and within the silicon oxide region; and three (d)–(f) at various poly-Si locations. The purpose of these scans was to explore the capabilities of PTR for measuring recombination lifetimes in and around scribeline locations with the goal of using these values as very convenient benchmarks for wafer contamination monitoring during (or after) processing.

Fig. 4 shows the PTR frequency amplitude and phase obtained at the six locations of Fig. 3: three scans (open symbols) were performed through the oxide layer outside the scribeline (points (a)–(c) in Fig. 3); and three more scans (solid symbols) on three poly-Si pads of different sizes and 4500-Å thickness scribeline (points (d)–(f) in Fig. 3). One scan was performed inside the scribeline (point b on the straight line A in Fig. 3). Continuous lines (over the open symbols) represent the multi-parameter best fits of the experimental data for SiO_2 locations using a 3-D PTR model [7,8]. Point (d) lies inside a small poly-Si pad (150×150 μm) close to the scribe line. Point (e) lies inside a larger poly-Si pad (300×300 μm). Finally, point (f) lies inside a wide poly-Si strip perpendicular to the investigated scribeline. It is interesting to see that the PTR signals from these poly-Si regions exhibit different behavior in Fig. 4. The smallest pad (d) and the intermediate size pad (e) exhibit both thermal and carrier plasma behavior, with the free-carrier contributions clearly appearing at frequencies > 500 Hz. On the other hand, the poly-Si strip (f) exhibits purely thermal contribution throughout the entire frequency range 10 Hz–100 kHz. These systems consist of three layers (Si substrate + gate SiO_2 + poly-Si). For this reason, it was not possible to fit the experimental data using our 3D-PTR model, which predicts the response of a single-layer Si wafer. An extension of the single-layer PTR model to electronically active multi-layers along the lines of our earlier theoretical treatment of modulated thermoreflectance signals from similar geometries [9] is currently under development. The fact that the responses of these three poly-Si layers were different may be likely due to the increasingly greater depletion of the photoexcited free carrier contribution with increasing lateral dimensions of the layer. Earlier work [10] showed that lifetime measurements through poly-Si layers in MOS capacitor structures are possible, since any photoexcited carrier within the Si substrate can emit infrared radiation through the pad, which can be captured by the PTR detection electronics. Under this hypothesis, scattered light propagating across a small-size poly-Si pad can eventually penetrate the oxide-Si underlayer and generate carriers, thus creating the partly plasma-wave scan of Fig. 4, curves (d) and (e). As the lateral dimensions of the poly-Si layer increase, the probability of the essentially spherically propagating scattered photons reaching the substrate diminishes due to the increased lateral (radial) scattering in the polysilicon. As a result, more of the incident optical power is converted readily into heat within the poly-Si layer, creating the purely thermal scan of Fig. 4, curve (f). This purely thermal behavior of the strip (f) is consistent with the expected very high optical-to-thermal (nonradiative) conversion efficiency of the laser radiation in the presence of a very

Table 1
Electronic and thermal parameters for three points located across the scribeline (Fig. 3)

Location	Amplitude (mV)	α (cm^2/s)	τ (μs)	D_n (cm^2/s)	S_1 (cm/s)
a	10.613	0.55	36	2.0	440
b	10.475	0.55	35	2.4	630
c	9.730	0.55	35	2.0	600

high density of free thermal carriers within the poly-Si layer (nearly metallic behavior). Clearly, more theoretical and experimental work is needed to understand quantitatively the mechanism of the PTR signal generation from deposited poly-silicon layers on gate oxides. The important issue of the influence of adjacent poly-Si layers/pads on scribeline PTR signals similar to those in Fig. 4 is further discussed in section 4.3 below.

Electronic parameters for the probed SiO_2 locations (a)–(c) are shown in Table 1. According to these results the SiO_2 regions inside and around the scribeline exhibit the same lifetime (~35 μs), without any great variations in the values of the carrier diffusion coefficient. Surface recombination velocity S_1, however, does vary substantially as a function of location. No transient behavior was found in any of the examined locations, thus indicating good quality surfaces with low surface defect state densities, as expected from oxidized SiO_2–Si interfaces [3].

4.2. Thermoelectronic images

One region close to the central part of a wafer was scanned with a step of 20 μm, 300 × 340 μm in area (Region A in Fig. 1(a)), located near the center of the

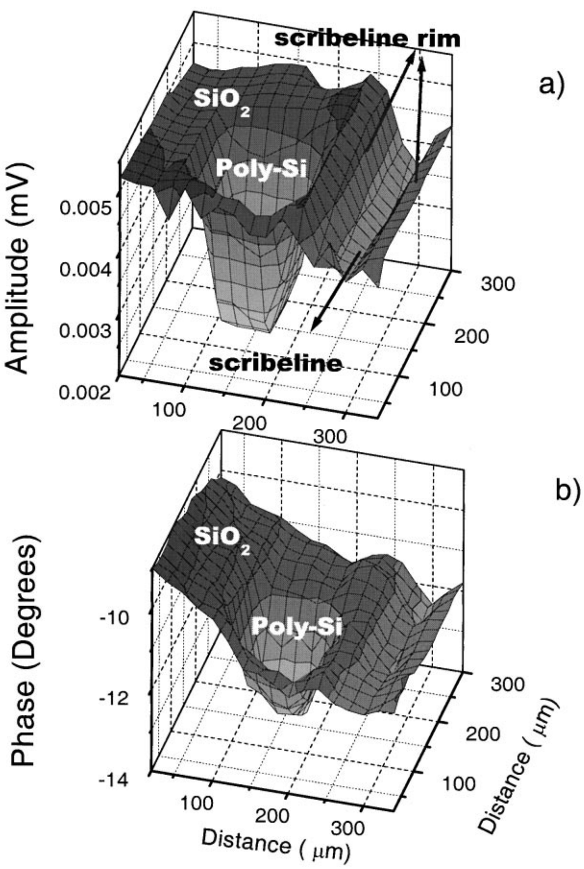

Fig. 5. PTR signal amplitude (a) and phase (b) thermoelectronic images for region A shown in Fig. 1(a).

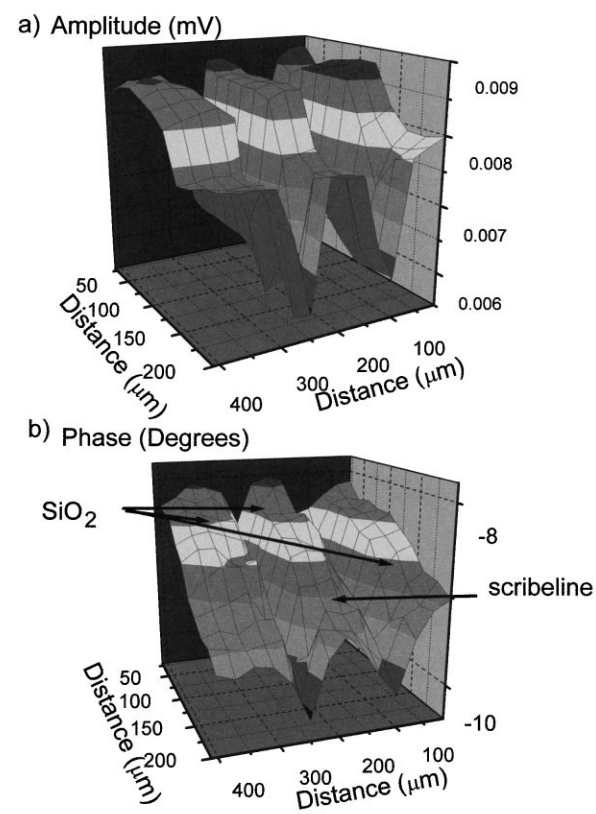

Fig. 6. PTR signal amplitude (a) and phase (b) thermolectronic images for region B shown in Fig. 1(a).

wafer. This region was chosen for PTR scanning imaging because it encompasses a square poly-Si test pad, a poly-Si scribeline rim, and half the width of a 120-μm wide scribeline. The PTR signal amplitude and phase images of this region obtained at the modulation frequency of 1 kHz are shown in Fig. 5(a) and (b), respectively. The low amplitude and large phase lag values correspond to the poly-Si regions, as expected from the efficient nonradiative conversion at this location leading to the absence of measurable photoexcited free-carrier densities and the domination of the signal by the thermal-wave component within the detection area of the infrared detector. On the other hand, high amplitude and small phase-lag values are associated with direct probing of the $Si–SiO_2$ interfaces, due to the domination of the PTR signal by the free-carrier plasma component. These results demonstrate that PTR imaging can be used to identify areas of high and low electronic activity across a particular patterned region of a processed wafer. It is important to note that neither the amplitude nor the phase levels inside the half-scribeline image are equal to those from the oxide patches outside the scribeline. We will return to this important point below.

A scribeline junction (120-μm thickness), approximately 2 cm radially away from the wafer flat (region B in Fig. 1), was also scanned. The imaged area, 400 × 200 μm across the wide scribeline, was scanned as delineated at 1 kHz with a 20-μm step. Following preliminary exploratory scans, the purpose of this scan was to investigate the apparent effects on the PTR signal of the proximity of poly-Si pads to probed oxide layers. Therefore, the scanned area was confined within the delineated perimeter. It included the two parallel poly-Si rim lines on both sides of the scribeline, and the oxidized areas outside the scribeline. The amplitude image (Fig. 6(a)) of this area exhibits deep grooves (representing the straight parallel poly-Si rims of the scribeline) on both sides of the central line, which represents the signal from inside the scribeline. The back portion of the image borders the region close to the crossing point of this scribeline with the perpendicular scribeline. The signal strength decreases and the phase lag increases in the vicinity of the two frontal poly-Si pads. It was speculated that this phenomenon may be due to enhanced recombination following photoexcited carrier diffusion in the neighborhood of the heavily doped pads, as the laser beam approached the borders of the two pads within an ac electronic diffusion length, $L = (D\tau)^{1/2}/(1 + \iota\omega\tau)$ [8]. Of further interest in this PTR image is that both amplitude and phase images *inside the scribeline* show the same trends as those scanned on the oxide *outside the scribeline*, even though the scribeline is not in the immediate vicinity of the pads. Further line scans (lines (A)–(C); see Fig. 3) inside and alongside the entire length of this scribeline (see section 4.3) showed that the ac diffusion length is approximately 100 μm in this region. This is of the order of the distance of the pads from the adjacent scribeline regions and corroborates the possibility of the influence of the pad structure on the recombination mechanism of diffusing photoexcited carriers.

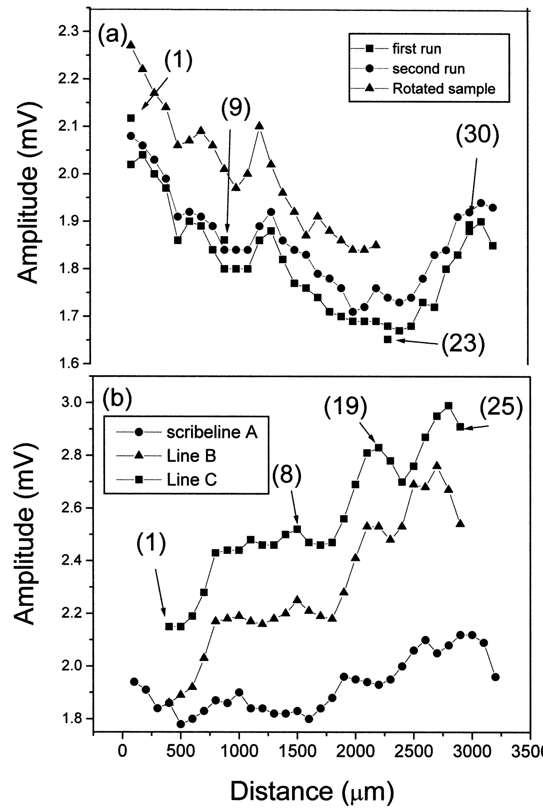

Fig. 7. (a) PTR signal amplitude line scans inside of a typical scribeline located at the central part of the wafer. (b) Three PTR amplitude line scans for lines (A)–(C) as shown in Fig. 3.

4.3. Study of poly-Si structure effects on PTR signals through line scans

To further probe potential interaction effects between the electronic properties inside scribelines and the adjacent poly-Si pads on the PTR signal, it was decided to perform single-line scans in two different locations on the patterned wafer: (a) a full-length scan inside the insert-free scribeline located in the central part of the wafer; and (b) three full-length scans at a location elsewhere on the wafer, with structures very similar to those shown in the CCD image of Fig. 3. In each scribeline location thirty points/line were probed. Total length was 3000 μm. In the latter case the equivalents of lines (A)–(C) in Fig. 3 were scanned. Fig. 7(a) shows signals from two line scans inside the typical scribeline located in the central part of the wafer, carried out in two directions: first from point 1 to point 30; then from point 30 to point 1. The results were obtained using a 100-μm step with the waist of the Gaussian laser beam scanned along the center of the scribeline. Optical alignment was ensured by using the CCD camera, while moving two micrometer stages in conjunction with scan corrections through slight sample rotations. Finally, in order to offset systematic errors to the measurement due to possible inclinations of the plane of the wafer with respect to the laser beam leading to defocusing, the sample was rotated about 30° and the same scan was performed. It is seen that the PTR signal amplitude shows some variation along the scribeline. It is noted that the forward- and reverse-direction scans produced very similar patterns. The same is true (within a constant multiplication factor) for the scan profile inside the scribeline of the rotated sample. The trends can be correlated to the three large poly-Si pad structures similar to pads P1–P3 shown in Fig. 3: the closer the laser beam gets to these outside pads, the smaller the signal amplitude becomes. When the beam is sufficiently away from the three large-pad region, the signal recovers. The laser beam, however, keeps scanning alongside a series of small poly-Si pads on both sides of the scribeline. Accordingly, the PTR amplitude recovery is not at the same level as at the starting point (1) (see Fig. 7(a)). This point exhibits the strongest PTR amplitude and is most remote to any kind of poly-Si pad (point (b) in Fig. 3). Four points located inside this same scribeline were subsequently examined in greater detail: point ♯1 at a distance of 100 μm away from the perpendicular crossing scribeline; point ♯9 at 900 μm; point ♯23 at 2300 μm; and point ♯30 at 3000 μm.

Another scan was carried out in and alongside the scribeline of Fig. 3, located far away (~2 cm) from the wafer center (lines (A)–(C) equivalent in Fig. 3). Fig. 7(b) shows the three PTR signals at 1 kHz. The PTR signals in the vicinity of poly-Si pads follow the trends observed in Fig. 7(a), with maximum amplitude suppression in the neighborhood of the three large poly-Si pads to the right of the scribeline, followed by gradual signal recovery away from those pads. In this case, the signal along line (B) (closest to the large pads) is consistently smaller than that along line (C), which lies farther away, but closer to a set of smaller poly-Si pads on its right. The signal (A) inside the scribeline is the weakest of all three scans as the laser beam passes alongside the three large pads, but is always close to arrays of smaller pads lying on both sides of the scribeline. Nevertheless, all three signals recover as the laser beam moves sufficiently away from the large pads and from the smaller pads immediately below point ♯15 at 1500 μm distance from the top of the scan. Finally, the signal amplitude inside the scribeline (A) decreases rapidly as the laser beam approaches the horizontal junction at the bottom with the wide poly-Si strip, offering further clear evidence of the detrimental effect on the PTR signal of large poly-Si covered areas in the vicinity of the scan. Similar, but proportionately smaller, effects are seen for line scans (B) and (C) as they approach the narrow horizontal poly-Si structures lying just beyond point ♯25. Frequency scans were performed at four points located in the scribeline (C), Fig. 3, at locations ♯1 (300 μm away from the upper transverse scribeline); ♯8 (1100 μm); ♯19 (2200 μm); and ♯25 (2800 μm) and at two more points across of the three lines (M) and (N).

Four points located in the scribeline at the central part of the wafer were scanned. Relative signal amplitude trends at 1 kHz are consistent with the scribeline scans of Fig.7(a). The electronic and thermal transport parameters calculated from multi-parameter fits at these points are shown in Table 2. Once again, as in the case of the scribeline scan in Fig. 3, a most significant finding is that recombination lifetime values remain constant (40 μs) along the scribe line, while changes in the front surface recombination velocity (and carrier diffusion coefficient to a lesser extent) were found. These lifetime values are slightly different from those obtained inside the scribeline located near the center of the wafer. Our recent work [7] has shown that substrate lifetimes are likely to vary across the surface of 4″ and 6″ wafers. Given the strong near-surface absorption of the laser beam at 514 nm (optical

Table 2
Electronic and thermal parameters for four points located along a scribeline located near the center of the wafer

Location	Amplitude (mV)	α (cm^2/s)	τ (μs)	D_n (cm^2/s)	S_1 (cm/s)
Point 1	3.641	0.55	40	3.0	420
Point 9	3.394	0.55	40	2.8	280
Point 23	3.4241	0.55	40	2.8	280
Point 30	3.577	0.55	40	2.6	350

Table 3
Electronic and thermal parameters for six points located as shown in Fig. 3

Location	Amplitude (mV)	α (cm^2/s)	τ (μs)	D_n (cm^2/s)	S_1 (cm/s)
Point 1	3.7342	0.55	22	2.5	260
Point 8	3.8819	0.55	22	4.0	185
Point 19	3.9751	0.55	22	7.0	160
Point 25	3.9220	0.55	22	8.0	120
M	3.6013	0.55	22	2.5	130
N	3.7545	0.55	22	2.6	133

absorption depth ~1 μm from the surface), it is reasonable to expect that the affected parameter in the presence of adjacent poly-Si pads is the surface recombination velocity, rather than the bulk recombination lifetime. In fact, the surface recombination velocity does carry implicit information on the surface recombination lifetime [7] due to the density of electronic states or other perturbations there, such as highly doped polysilicon regions within a diffusion length from poly-Si pads.

Signals from four points along line (C) Fig. 3 and the two additional points (M) and (N) were obtained and best-fitted to the theory using the 3-D PTR model [8]. Electronic and thermal transport parameter values for all points are reported in Table 3. In agreement with prior results, the recombination lifetime remains constant along the length of the scribeline, whereas strong changes are observed in the carrier diffusion coefficient and the surface recombination velocity: The former increases at scribeline locations far away from the large poly-Si pads; the latter decreases in these regions, as intuitively expected from enhanced near-surface recombination in the neighborhood of the highly doped pad regions.

5. Conclusions

The present work establishes the use of PTR frequency scans at any point inside the scribeline of a processed Si wafer, as a reliable, quantitative measure of the substrate recombination lifetime. This, in turn, may be used to monitor the integrity of the in-line process, such as furnace contamination, substrate thermal cycling fatigue, dislocation propagation and defect creation, etc. Owing to perturbations of the signal by poly-Si pads around a given scribeline, it is recommended that laser probing should be done at locations as far as possible from such pads. The presence of poly-Si pads, however, does *not* affect the value of the bulk recombination lifetime. It only affects the surface recombination velocity and/or the diffusion coefficient. The actual location of the scribeline on the wafer surface may affect the value of the lifetime. This is so, because lifetimes are known to vary across the surface of Si wafer substrates [7]. Any Si-wafer metrologic technology is limited by these variations to a larger or lesser extent. A solution is for PTR probing to be performed at approximately the same coordinate location on a given set of wafers from the same vendor. This is easily achieved with mechanical/robotic positioning of the laser beam for on- or off-line inspections. The sensitivity of the PTR signal to the size of poly-Si pads may be a useful tool for monitoring the mechanical and electronic quality of the poly-Si deposition process.

Acknowledgements

The authors would like to acknowledge the support of Materials and Manufacturing Ontario (MMO) for this industrial research and development project. One of the authors (MER) wishes to acknowledge CICATA (México) and COLCIENCIAS (Colombia) for their partial support.

References

[1] Van Zant P. In: Microchip fabrication. New York: McGraw-Hill, 1997. p. 102.
[2] Mandelis A. Solid-State Electron 1998;42(1):1.
[3] Rodriguez ME, Garcia JA, Mandelis A, Jean C, Riopel Y. Appl Phys Lett 1999;74:2429.
[4] Salnick A, Mandelis A, Jean C. Appl Phys Lett 1997;71:2671.
[5] Salnick A, Mandelis A, Jean C. Phys Stat Solidi (a) 1997;163:R5–R6.
[6] Salnick A, Mandelis A, Ruda H, Jean C. J Appl Phys 1997;82:1853.
[7] Rodriguez ME, Mandelis A, Pan G, Nicolaides L, Garcia JA, Riopel Y. J Electrochem Soc (in press) 1999.
[8] Ikari T, Salnick A, Mandelis A. J Appl Phys 1999;85:7392.
[9] Christofides C, Diakonos F, Seas A, Christou C, Nestoros M, Mandelis A. J Appl Phys 1996;80:1715.